SSRG International Journal of Electronics and Communication Engineering
ISSN: 2348-8549/ https://doi.org/10.14445/23488549/IJECE-V11I2P105

Volume 11 Issue 2, 41-49, February 2024

Original Article

Multiport Shared Radiator for Signal Transmission of 5G Millimeter Wave Application

Neetu Agrawal[1], Sanjay Chouhan[2], Manish Gupta[3]

[1,3]*Department of Electronics and Communication Engineering, GLA University, Uttar Pradesh, India.*
[2]*Department of Electronics and Communication Engineering, Jawaharlal Institute of Technology, Madhya Pradesh, India.*

[1]*Corresponding Author : neetuagrawal.ec@gla.ac.in*

Received: 27 October 2023 Revised: 02 December 2023 Accepted: 27 December 2023 Published: 02 February 2024

Abstract - *In the world of wireless communication, antennas are essential components. Antennas act as a link between electrical devices and the intangible waves that transmit data over various communication systems. Meandered line antennas have several benefits, including proven impedance matching, multiband operation, and compact size. For millimeter-wave 5G communication, a Multiple-Input Multiple-Output (MIMO) antenna with Meander lines sharing a radiator is described. The single element radiator's unique design offers the required isolation; it doesn't use isolation techniques to enhance isolation. In addition, the isolation is further improved by the orthogonal placement of ports with a ring-shaped partial ground structure. In the operational frequency range of 15.74-34.88 GHz, the achieved isolation is more than 13 dB. This design is more compact since all the radiating parts are positioned extremely near one another. The suggested antenna is constructed on a Rogers RT5880 substrate, measuring 30 x 30 x 0.8 mm^3. A few other important MIMO performance parameters that are assessed are far-field gain, Diversity Gain (DG), Mean Effective Gain (MEG), Channel Capacity Loss (CCL), and Envelope-Correlation Coefficients (ECC). It is found that the MEG < -2.2 dB, ECC < 0.007, CCL < 0.4 bit/s/Hz, and DG > 9.97 dB satisfy the requirements. Over the operational band, a peak gain of 7.5 dB is attained. The radiation and total efficiency are more significant than 62% and 85% in the operational band, respectively. These measured and simulation-derived values show good agreement, suggesting that the antenna fits 5G applications.*

Keywords - *MIMO, 5G, Isolation, ECC, MEG.*

1. Introduction

Utilizing multiple antenna approaches is crucial in contemporary wireless communication systems, yielding enhanced error performance and increased data rates at the expense of increased network complexity and costs. Compared to a Single-Input Single-Output (SISO) antenna system, a MIMO system offers more channel capacity without increasing broadcast power or spectral bandwidth.

A successful MIMO antenna system should minimize mutual coupling between the antennas. Maintaining high isolation between antennas is the primary design constraint in MIMO antennas [1, 2]. Antenna researchers have reported on various MIMO antenna designs for 5G wireless use with better isolation among antennas [3, 4]. Compared to the 4G system, the 5th Generation (5G) technology may offer several benefits, including a more significant transfer rate and lower latencies [5-8]. 5G spectrum can be found in lower frequency band (Sub-6GHz) and higher frequency band (mm-wave).

Furthermore, concentrating on the mm-wave frequencies (more than 6 GHz) has presented particular difficulties for 5G technology. The mm-wave frequency band signal can travel a few miles due to attenuation loss [9]. Meanwhile, this challenge is being overcome by building a directional antenna with a high gain [10, 11].

For different countries, there are three distinct 5G sub-6 GHz frequency bands: 3.3–4.2 GHz, 4.4–4.9 GHz, and 5.15–5.925 GHz. The 5G millimeter-wave frequencies are as follows: 24.2 GHz - 27.5 GHz, 26.5 GHz - 27.5 GHz, 37 GHz - 37.6 GHz, and 37.5 GHz - 42.5 GHz. A significant number of MIMO antennas for 5G applications in the mm-wave and sub-6 GHz frequency ranges have been made public by the researcher.

In this work, a handful of these are discussed. The reported multiband MIMO antenna design includes WLAN bands and 5G sub-6 GHz bands [12]. A U-shaped 4-element MIMO antenna is designed for a 5G lower spectrum. The operating band is 3.2-3.84 GHz. Isolation between ports of more than 14 dB was achieved using a decoupling structure in the middle of the radiating element and a separate partial ground structure. A multi-port single antenna with many cuts

is introduced for the WLAN application. To improve the isolation of the designed antenna, ports are arranged in an orthogonal mode.

A square shape slotted millimeter-wave antenna array has been introduced. The antenna size is compact, and the operating frequency band is 36.5 - 40.2 GHz. A patch antenna design provides new opportunities for 5G services at 38 GHz band ranges from 37-40 GHz [13]. A High-performance dual-polarized antenna is designed.

The designed antenna is inclined to use most of the international commercial 5G mm-wave frequency bands [14]. A thorough review of the 5G MIMO antenna and its application is done. It examines the progression of the spectrum towards 5G, which encompasses the mm-wave band and sub-6 GHz frequency band, as well as its benefits and drawbacks [15]. A fragment-shaped antenna design with improved isolation is reported for lower sub-applications [16]. Compact antenna design is a significant challenge in devices with less mutual coupling by MIMO techniques. Miniaturization is easy using a Common-Element (CE) antenna structure.

This research proposes a four-port meander, line single element radiator with -10 dB bandwidth 15.74-34.88 GHz. The proposed antenna resonates at 19.5 GHz, which is suitable for K-band satellite applications and defense systems [29, 30]. The proposed single radiator is self-isolated; no decoupling technique or component is required to limit the effects of mutual coupling between various antenna ports; instead, the antenna form alone provides more than 13 dB of isolation. In this design, four-port antenna elements on the substrate are connected in such a way as to form a single component, and a rectangular ring-shaped ground plane reduces the size of the presented design.

2. Antenna Design

Any antenna design necessitates careful observation and analysis. The MIMO antenna is 30 x 30 x 0.8 mm^3 in total. It covers the mm-wave spectrum and offers a -10 dB impedance bandwidth of 15.74-34.88 GHz. Figures 1 and 2 show the suggested MIMO antenna's antenna design geometry and fabrication views.

Table 1 shows dimensions that have been optimized. It has a common ground plane of Perfect Electrical Conductor (PEC) material. In the proposed MIMO antenna construction, each element is coupled to the other and uses a single ground plane. The four radiating patches that comprise the proposed MIMO antenna are joined to form a single radiating element, excited by a microstrip feedline and a ring-shaped rectangular ground plane. A rectangular ring ground plane was used to help reduce size and improve the isolation of the proposed MIMO antenna.

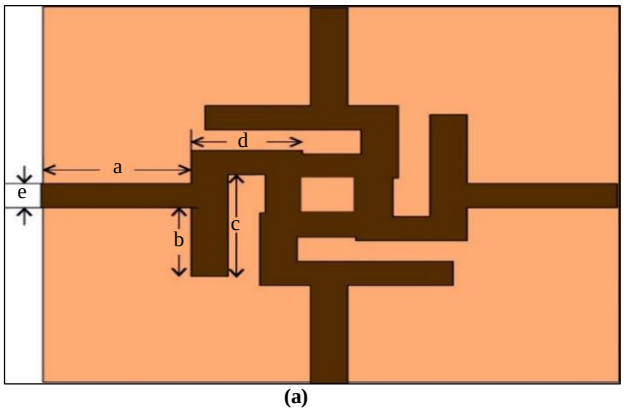

(a)

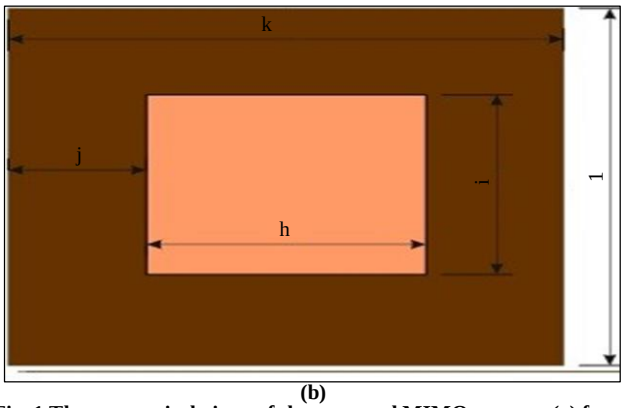

(b)

Fig. 1 The geometrical views of the proposed MIMO antenna (a) front, and (b) back.

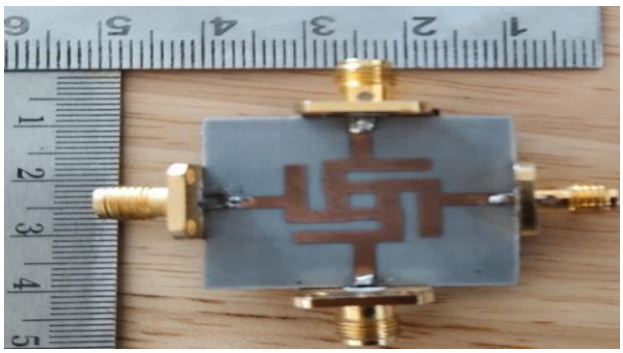

(a)

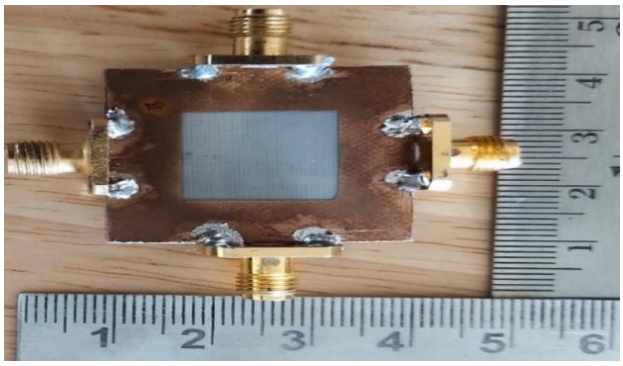

(b)

Fig. 2 Proposed MIMO antenna fabrication views (a) Top view, and (b) Bottom view.

Table 1. Optimized dimension

Antenna Parameters	a	b	c	d	e	h	i	j	k	l
Size (mm.)	8.0	5.0	8.0	6.0	2.0	15	15	7.7	30	30

3. Design Steps of the Proposed

Figure 3 shows the proposed MIMO antenna design processes. A step-by-step process designs the proposed antenna. The meander line structure provides better size reeducation as compared to other techniques. In step 1, a 50-ohm meander line is formed. Similarly, meander line antennas are produced in steps 2, 3, and 4.

Figure 4 shows the simulated design steps S parameter (S11) result. Design Step 1 (DS 1) does not produce any resonance, while DS 2 produces better results and the desired resonance. DS 3 and DS 4 both give better results and wide bandwidth. The proposed antenna (Design Step 4) provides better return loss and sharp resonance than others.

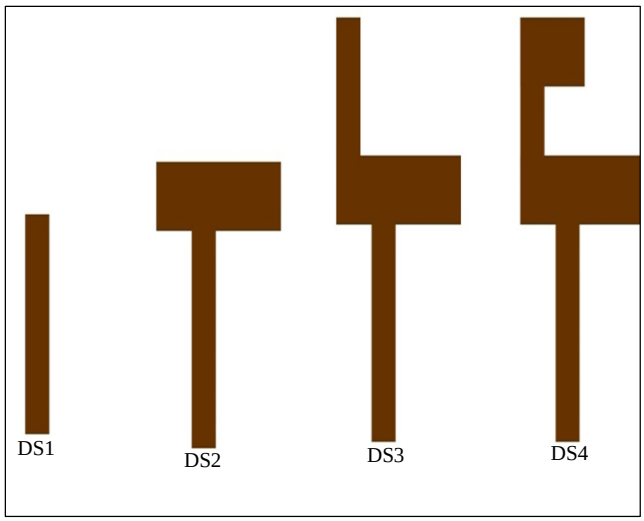

Fig. 3 Proposed antenna Design Steps (DS)

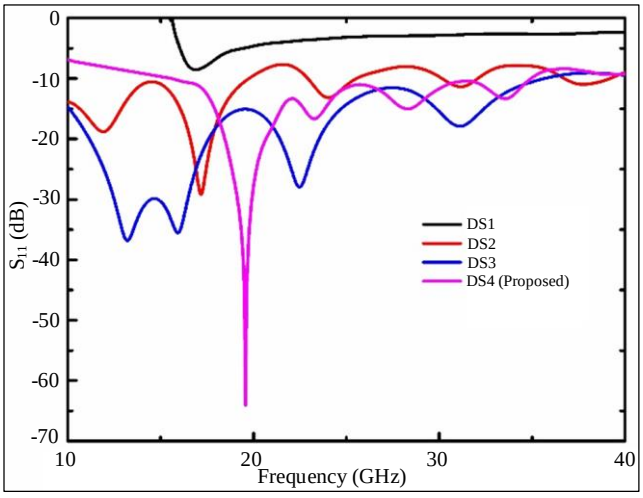

Fig. 4 Simulated S-parameters (S_{11}) Design Steps result

4. Materials and Methods

Any antenna design necessitates careful observation and analysis. Antenna design is also significantly influenced by the fabrication material. CST microwave studio is used to design and optimize the suggested antenna. The substrate used for the described antenna is Rogers RT5880, which has a loss tangent of 0.009 and a relative permittivity of 2.2. Although expensive, dielectric materials have a low loss.

5. Results and Discussion

The proposed MIMO antenna's S-parameters are simulated and measured using the Vector Network Analyzer (VNA) and CST Studio Suite software. The isolation coefficient and return loss are examined using S-parameters. The simulated design steps S parameter (S11) outcome is displayed in Figure 4. While Design Step 2 yields better results and produces the intended resonance, Design Step 1 (DS 1) does not produce any resonance. Both DS 3 and DS 4 offer greater performance and a large bandwidth. Compared to other antennas, the suggested antenna (Design Step 4) provides superior return loss and acute resonance. The measured and simulated S-parameters for port 1 are displayed in Figure 5. S11 stands for the return loss coefficient, whereas S21, S31, and S41 stand for the isolation coefficients.

Figure 5 shows that the observed frequency range of the proposed MIMO antenna is 15.9-35 GHz, whereas the simulated -10 dB frequency range is 15.74-34.88 GHz. The observed and predicted resonance frequencies of the proposed MIMO antenna are 20 GHz and 19.56 GHz, respectively. The measured and simulated return loss at resonance are almost identical. There are small variations between the measured and simulated measurements due to manufacturing flaws.

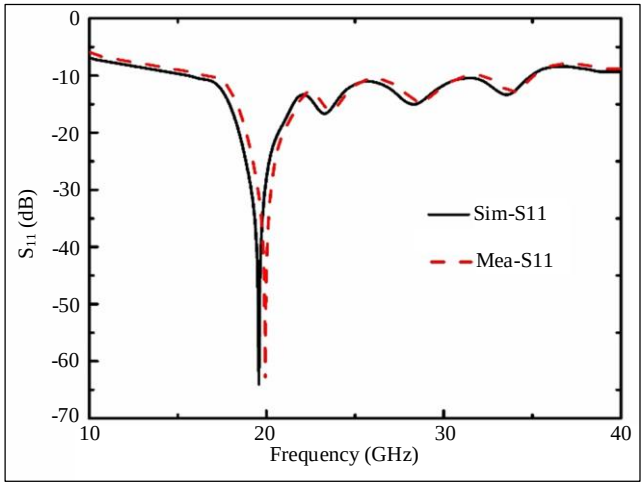

(a)

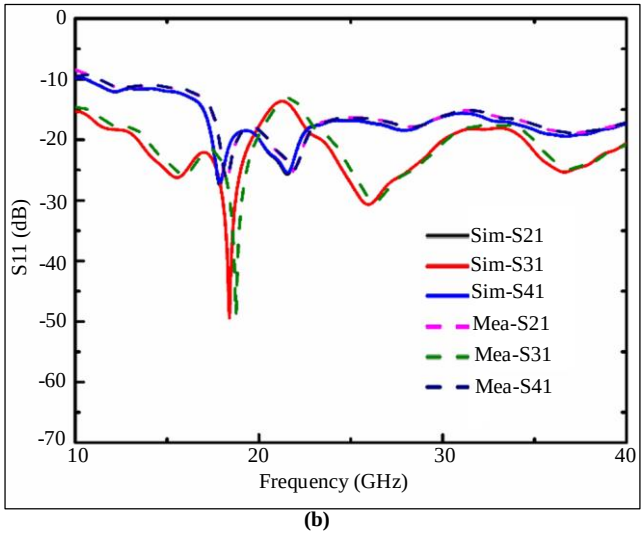

(b)

Fig. 5 Measured-simulated S- parameters (a) S11, and (b) Isolation coefficients.

Fig. 6 Measurement setup

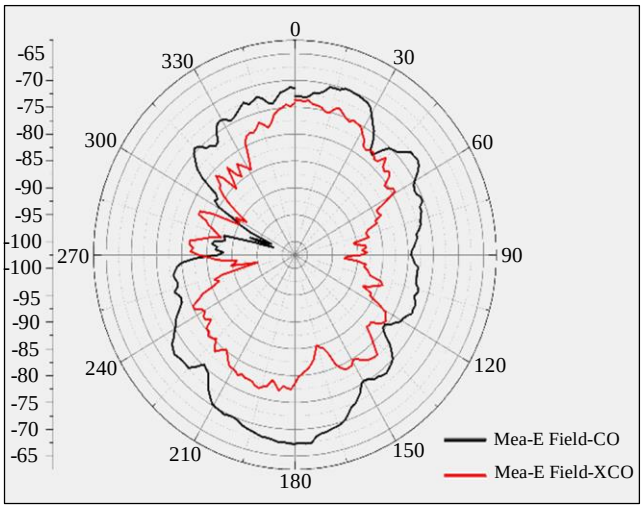

(a)

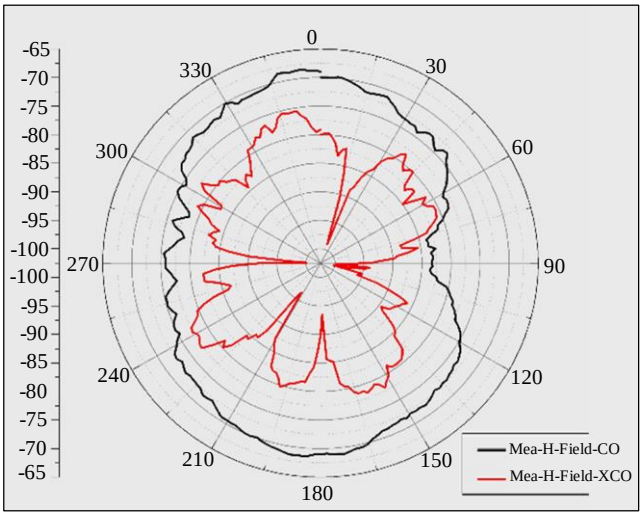

(b)

Fig. 7 Far field pattern (a) E plane, and (b) H plane.

The VNA measurement configuration for S-parameters and far-field gain is displayed in Figure 6. The prototype system underwent extensive field testing for radiation patterns in both the H and E planes. Additionally, an antenna was positioned vertically and horizontally in an anechoic environment using positioning tools to assess the E and H-plane values. The E-plane for 0 degrees and the H-plane for 90 degrees have been provided to show the antenna's radiation pattern. Figure 7 displays the normalized radiation patterns of the E and H planes as observed and simulated. The E-field's primary lobe direction is 330 degrees, and its magnitude is 20.5 dBV/m. Similarly, the direction and magnitude of the major lobe of the H-field are 0 degrees and 34.3 dBA/m. The observed and simulated far-field gain concerning frequency is shown in Figure 8. Far-field gain is simulated and measured using the CST tool in an anechoic room. The estimated gain is 3-7.5 dB, while the affected gain is between 4.5 and 5.9 dB within the frequency spectrum.

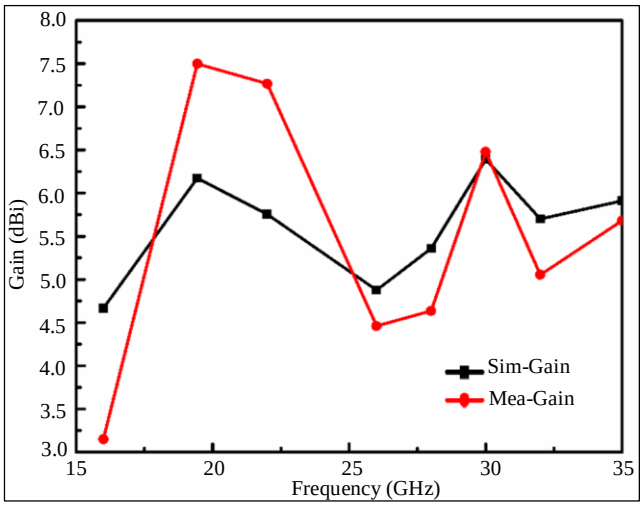

Fig. 8 Simulated and measured far-field gain

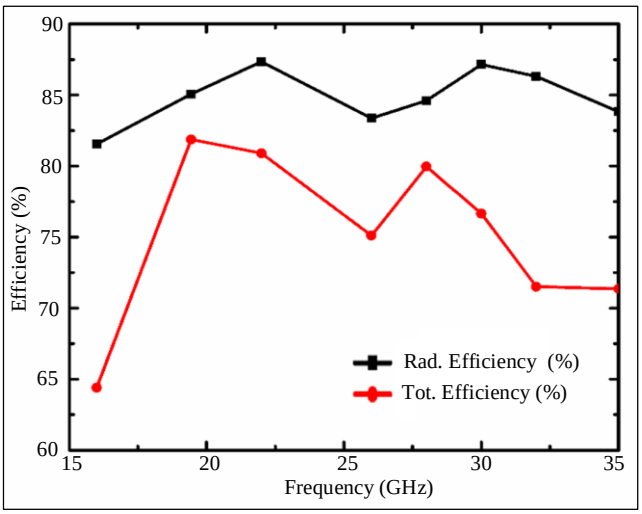

Fig. 9 Radiation and total efficiency

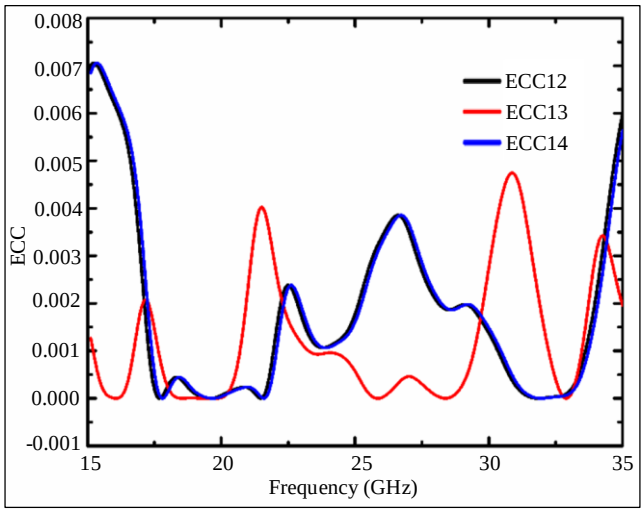

Fig. 10 Envelop Correlation Coefficient

The simulated and measured gains are 6.1 and 7.5 dB at resonance frequency, respectively. As depicted in Figure 9, the band's radiation efficiency and total efficiency are higher than 82% and 62%, respectively. The ECC denotes the relationship among antenna elements and can be calculated using S-parameters. ECC is critical because separate isolation measures cannot present the diversity response. The calculation of ECC is done by given Equation (1).

$$|\rho_e(l,m,N)| = \frac{|\Sigma_{n=1}^{N} S_{l,n}^{*} S_{n,m}|}{\sqrt{\left|\Pi_{k(=l,m)}\left[1-\Sigma_{n=1}^{N} S_{l,n}^{*} S_{n,k}\right]\right|}} \quad (1)$$

Where the total number of antennas is N and the antenna elements are l and m. Equation (2) can be used to calculate (ρ_{e12}) for two ports:

$$\rho_{e12} = \frac{|S_{12}S_{11}+S_{22}S_{21}|^2}{(1-|S_{21}|^2-|S_{11}|^2)(1-|S_{12}|^2-|S_{22}|^2)} \quad (2)$$

Where S_{11} is the return loss coefficient at port 1, and S22 is the coefficient at port 2. In addition, S_{12} and S_{21} are isolation coefficients between port 1 and port 2. Likewise, ECC is used to examine the impact of coupled return-loss and isolation parameters. Figure 10 depicts ECC results. The ECC is below 0.007 in the whole simulated frequency spectrum, showing that MIMO exhibits successful diversity results. The result of ECC, 0.007, signifies that there is very little correlation between the antenna array. ECC12, ECC13, and ECC14 represent the ECC between ports.

Figure 11 displays the proposed MIMO antenna DG. The DG > 9.95 dB in the whole frequency spectrum. Likewise, DG can be computed by Equation 4 [2], which shows it is affected by correlation (ρ_e). The ideal value of DG is 10dB. The higher the DG, the lower the correlation value.

$$G_{DG} = 10 \times \sqrt{1-|\rho_e|^2} \quad (3)$$

MIMO antenna diversity features can also be demonstrated using the MEG. The MEG is explored for the Isotropic and Gaussian mediums to test the diversity performance for various Cross-Polarization Ratios (XPR). Figure 12 shows the MEG value for the Isotopic and Gaussian medium. The MEG is uniform or constant for an isotropic medium of -3dB in the whole operating band at XPR =0 dB, whereas at XPR 6dB, MEG varies from -2.34 to -2.11 dB.

Similarly, MEG for Gaussian medium ranges from -6.24 to -3.82 dB at XPR=0 dB and from -5.81 to -2.51 dB at XPR=6 dB. Table 2 shows comparisons of MEGs for both mediums at resonance frequency. The MEG is used to determine each antenna's overall received strength. Equations (4) and (5) are used to observe it for applications both indoors at XPR= 6 dB and outdoors at XPR = 0 dB.

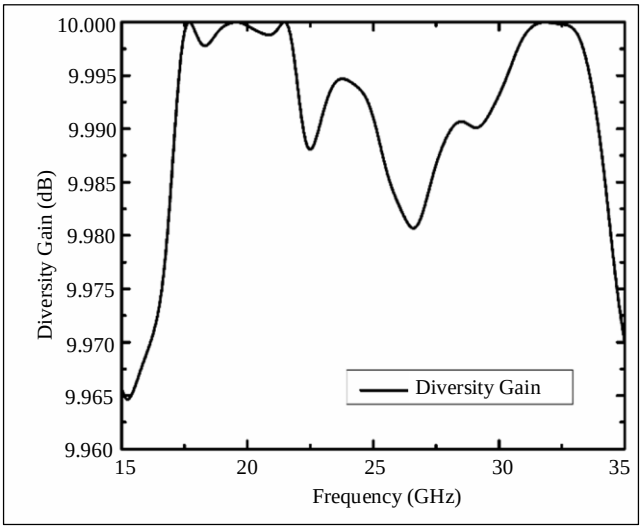

Fig. 11 Proposed antenna diversity gain

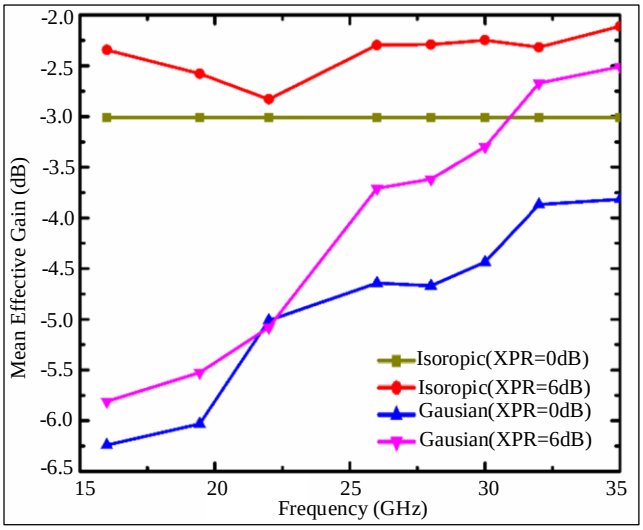

Fig. 12 Proposed antenna MEG

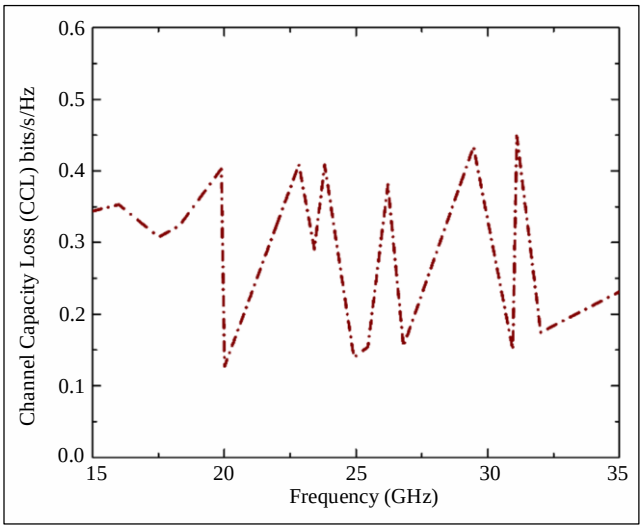

Fig. 13 Channel capacity loss

$$\mathrm{MEG}_i = \&\frac{P_{\mathrm{rec}}}{P_{\mathrm{inc}}} = \oint \left[\frac{\mathrm{XPR}\cdot G_{\theta i}(\Omega)+G_{\phi i}(\Omega)\cdot P_{\phi}(\Omega)}{1+\mathrm{XPR}}\right] d\Omega \quad (4)$$

$$\mathrm{MEG}_i = \int_0^{2\pi}\int_0^{\pi}\left(\frac{\mathrm{XPR}}{1+\mathrm{XPR}}\mathrm{G}_{\theta}(\theta,\emptyset)\mathrm{P}_0(\theta,\emptyset) + \frac{1}{1+\mathrm{XPR}}\mathrm{G}_{\emptyset}(\theta,\emptyset)\mathrm{P}_{\emptyset}(\theta,\emptyset)\right)\sin\theta d\theta d\emptyset \quad (5)$$

Table 2. MEG results at the resonance frequency

MEGs	Isotropic Medium	Gaussian Medium		
	XPR at			
Resonance Frequency (GHz)	0 dB	6dB	0dB	6dB
19.50	-3.0 dB	-2.80 dB	-6.0 dB	-5.50 dB

To provide information on the channel capacity losses of the system because of the influence of correlation, CCL was added to the MIMO characteristics. The CCL calculation was done using the following Equations: 6, 7, 8, and 9 [28]. It can be used to monitor system performance decline.

$$CCL = -\log_2 det(\eta) \quad (6)$$

Where η is the correlation matrix 2 x 2.

$$\eta = \begin{bmatrix}\sigma_{11} & \sigma_{12}\\ \sigma_{21} & \sigma_{22}\end{bmatrix} \quad (7)$$

$$\sigma_{ii} = 1 - \left(|S_{ii}|^2 - |S_{ij}|^2\right) \quad (8)$$

$$\sigma_{ij} = -\left(S_{ii}^* S_{ij} + S_{ji} S_{ij}^*\right) \quad (9)$$

Figure 13 shows a measured plot of the CCL over frequency. CCL must be lower than 0.4 bit/sec/Hz and achieve the desired CCL in the covered bands of operation, as illustrated in Figure 13.

Surface current can also be used to observe the effect of mutual coupling if port 1 was energized and rest ports were ended by 50 ohms matched impedance. Figure 14 depicts the proposed design's Surface Current Distribution (SCD) at 19.56 GHz. The partial ring shape ground at 19.56 GHz frequency is seen to have a comparatively low surface current.

Surface current has virtually little impact on the similar meander lines at other ports. It exhibits a lower current coupling with antenna elements 2, 3, and 4. The surface current ranges from 0 to 281 Ampere/m at various ports.

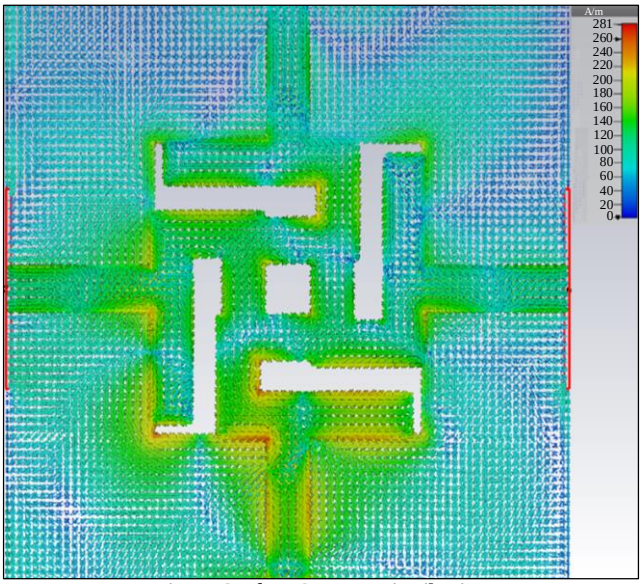

Fig. 14 Surface Current Distribution

Table 3. Comparison of the proposed MIMO antenna with the published work

Ref.	Bandwidth (GHz)	Complete Size (mm^2)	Isolation among Ports (dB)	ECC	Highest Gain (dB)	MEGs (dB)	Diversity Gain (dB)	CCL (bits/s/Hz)
[17]	26-29.7	30 x 30	>30	<0.0005	7.1	< -6	---	----
[18]	25.5-29.6	30 x 35	>10dB	<0.01	8.3	---	9.96	< 0.4
[19]	23-40	80 x 80	> 20	0.14	12	< -3	----	----
[20]	39-75	36 x 36	> 24.5	<0.00075	----	---	9.3	----
[21]	25-31	12 x 12	> 30	<0.015	11	---	9.91	0.19
[22]	24.10-27.18 33-44.13	24 x 20	> 16	<0.1	3	< -3	9.5	-----
[23]	27-29	30 x 30	> 29	<0.16	6.1	---	---	------
[24]	26.5-38.2	12 x 25.4	----	-----	6.8	---	---	------
[25]	25-33	19 x 19	> 25	<0.008	14.1	---	---	------
[26]	26-31	48 x 31	> 21	<0.0015	10	---	---	------
[27]	27.2-40	158 × 77.8	> 17	<0.001	7.2	---	---	------
[28]	24-38	110 x 55	> 24	<0.02	---	---	---	<0.4
Proposed Work	15.74-34.88	30 x 30	>13	<0.007	7.5	<-2.2	9.97	<0.4

The suggested 5G MIMO antenna is compared in Table 3 in terms of bandwidth, total size, isolation, ECC, MEG, and CCL. Compared to previously published antennas, the suggested antenna array is tiny, has a low ECC, offers high isolation, and has a peak gain of 7.5 dB. Its bandwidth is also broad.

6. Conclusion

For 5G mm-wave applications, a four-port single element radiator has been proposed. The resonance frequency of the suggested antenna design is 19.56 GHz, with a bandwidth range of -10 dB between 15.74 and 34.88 GHz. The suggested design's extremely low ECC < 0.007 indicates the reduced correlation between radiating parts. In the proposed design, four radiating elements are placed very close and connected to form a common component; hence, compactness has been achieved.

The isolation among ports is more than 13 dB using the rectangular ring-shaped ground plane. The measured gain > 3dB in the operating band. Additional antenna array performance parameters, including DG > 9.97 dB, CCL < 0.4 bits/s/Hz, and MEG ≤ -2.2 dB, have been documented across the operational frequency range.

The proposed MIMO antenna has better results from simulation and measurement, making it more appropriate for 5G applications that use a high-frequency spectrum.

References

[1] Poonam Tiwari et al., "Advancing 5G Connectivity: A Comprehensive Review of MIMO Antennas for 5G Applications," *International Journal of Antennas and Propagation*, vol. 2023, pp. 1-19, 2023. [CrossRef] [Google Scholar] [Publisher Link]

[2] Shailesh Jayant et al., "Decoupling Methods in Planar UltraWideband Multiple-Input-Multiple-Output Antennas: A Review of the Design, State-of-the-Art, and Research Challenges," *Electronics*, vol. 12, no. 18, pp. 1-22, 2023. [CrossRef] [Google Scholar] [Publisher Link]

[3] Ammar Armghan et al., "Sickle-Shaped High Gain and Low Profile Based Four Port MIMO Antenna for 5G and Aeronautical Mobile Communication," *Scientific Reports*, vol. 13, pp. 1-14, 2023. [CrossRef] [Google Scholar] [Publisher Link]

[4] Ajay Kumar Dwivedi et al., "Circularly Polarized Printed Dual Port MIMO Antenna with Polarization Diversity Optimized by Machine Learning Approach for 5G NR n77/n78 Frequency Band Applications," *Scientific Reports*, vol. 13, pp. 1-20, 2023. [CrossRef] [Google Scholar] [Publisher Link]

[5] Mohsen Attaran et al., "The Impact of 5G on the Evolution of Intelligent Automation and Industry Digitization," *Journal of Ambient Intelligence and Humanized Computing*, vol. 14, no. 5, pp. 5977-5993, 2023. [CrossRef] [Google Scholar] [Publisher Link]

[6] R. Delshi Howsalya Devi, R. Naresh, and C.N.S. Vinoth Kumar, "Advanced 5G Technology in Healthcare Field," *Resource Management in Advanced Wireless Networks*, 2023. [CrossRef] [Google Scholar] [Publisher Link]

[7] Jeffrey G. Andrews et al., "What will 5G be?," *IEEE Journal on Selected Areas in Communications*, vol. 32, no. 6, pp. 1065-1082, 2014. [CrossRef] [Google Scholar] [Publisher Link]

[8] Peng Wang et al., "Multi-Gigabit Millimeter Wave Wireless Communications for 5G: From Fixed Access to Cellular Networks," *IEEE Communications Magazine*, vol. 53, no. 1, pp. 168-178, 2015. [CrossRef] [Google Scholar] [Publisher Link]

[9] Wonil Roh et al., "Millimeter-Wave Beamforming as an Enabling Technology for 5G Cellular Communications: Theoretical Feasibility and Prototype Results," *IEEE Communications Magazine*, vol. 52, no. 2, pp. 106-113, 2014. [CrossRef] [Google Scholar] [Publisher Link]

[10] Mohsen Khalily et al., "Broadband mm-Wave Microstrip Array Antenna with Improved Radiation Characteristics for Different 5G Applications," *IEEE Transactions on Antennas and Propagation*, vol. 66, no. 9, pp. 4641-4647, 2018. [CrossRef] [Google Scholar] [Publisher Link]

[11] M. Abirami, "A Review of Patch Antenna Design for 5G," *2017 IEEE International Conference on Electrical, Instrumentation and Communication Engineering (ICEICE)*, Karur, India, pp. 1-3, 2017. [CrossRef] [Google Scholar] [Publisher Link]

[12] Yu-Ren Chen, and Wen-Shan Chen, "Design of MIMO WLAN 2.4/5.2/5.8 and 5G SUB-6 GHz Antennas for Laptop Computer Applications," *2020 International Workshop on Electromagnetics: Applications and Student Innovation Competition (iWEM)*, Makung, Taiwan, pp. 1-2, 2020. [CrossRef] [Google Scholar] [Publisher Link]

[13] Bilal Aghoutane et al., "Analysis, Design and Fabrication of a Square Slot Loaded (SSL) Millimeter-Wave Patch Antenna Array for 5G Applications," *Journal of Circuits, Systems and Computers*, vol. 30, no. 5, 2021. [CrossRef] [Google Scholar] [Publisher Link]

[14] Chisang You et al., "Wideband Dual-Polarized On-Board Antenna for 5G mmWave Mobile Application," *2022 14th Global Symposium on Millimeter-Waves & Terahertz (GSMM)*, Seoul, Korea, pp. 195-196, 2022. [CrossRef] [Google Scholar] [Publisher Link]

[15] Insha Ishteyaq, and Khalid Muzaffar, "Multiple Input Multiple Output (MIMO) and Fifth Generation (5G): An Indispensable Technology for Sub-6 GHz and Millimeter Wave Future Generation Mobile Terminal Applications," *International Journal of Microwave and Wireless Technologies*, vol. 14, no. 7, 2021. [CrossRef] [Google Scholar] [Publisher Link]

[16] Gorre Naga Jyothi Sree, and Suman Nelaturi, "Design and Experimental Verification of Fractal Based MIMO Antenna for Lower Sub 6-GHz 5G Applications," *AEU-International Journal of Electronics and Communications*, vol. 137, 2021. [CrossRef] [Google Scholar] [Publisher Link]

[17] Musa Hussain et al., "Design and Characterization of Compact Broadband Antenna and Its MIMO Configuration for 28 GHz 5G Applications," *Electronics*, vol. 11, no. 4, pp. 1-14, 2022. [CrossRef] [Google Scholar] [Publisher Link]

[18] Mahnoor Khalid et al., "4-Port MIMO Antenna with Defected Ground Structure for 5G Millimeter Wave Applications," *Electronics*, vol. 9, no. 1, pp. 1-13, 2020. [CrossRef] [Google Scholar] [Publisher Link]

[19] Daniyal Ali Sehrai et al., "A High-Gain and Wideband MIMO Antenna for 5G mm-Wave-Based IoT Communication Networks," *Applied Sciences*, vol. 12, no. 19, pp. 1-11, 2022. [CrossRef] [Google Scholar] [Publisher Link]

[20] Karrar Shakir Muttair et al., "A New Design of mm-Wave MIMO Antenna with High Isolation for 5G Applications," *International Journal of Microwave and Optical Technology*, vol. 16, no. 4, pp. 370-379, 2021. [Google Scholar] [Publisher Link]

[21] Niamat Hussain et al., "Metasurface-Based Single-Layer Wideband Circularly Polarized MIMO Antenna for 5G Millimeter-Wave Systems," *IEEE Access*, pp. 130293-130304, 2020. [CrossRef] [Google Scholar] [Publisher Link]

[22] Arpan Desai et al., "Compact Wideband Four Element Optically Transparent MIMO Antenna for mm-Wave 5G Applications," *IEEE Access*, pp. 194206-194217, 2020. [CrossRef] [Google Scholar] [Publisher Link]

[23] Mian Muhammad Kamal et al., "Infinity Shell Shaped MIMO Antenna Array for mm-Wave 5G Applications," *Electronics*, vol. 10, no. 2, pp. 1-12, 2021. [CrossRef] [Google Scholar] [Publisher Link]

[24] Manikonda Venkateswara Rao et al., "CSRR-Loaded T-Shaped MIMO Antenna for 5G Cellular Networks and Vehicular Communications," *International Journal of RF and Microwave Computer-Aided Engineering*, vol. 29, no. 8, 2019. [CrossRef] [Google Scholar] [Publisher Link]

[25] Niamat Hussain et al., "A Broadband Circularly Polarized Fabry-Perot Resonant Antenna Using a Single-Layered PRS for 5G MIMO Applications," *IEEE Access*, vol. 7, pp. 42897-42907, 2019. [CrossRef] [Google Scholar] [Publisher Link]

[26] Zamir Wani et al., "A 28-GHz Antenna for 5G MIMO Applications," *Progress in Electromagnetics Research Letters*, vol. 78, pp. 73-79, 2018. [CrossRef] [Google Scholar] [Publisher Link]

[27] Emad Al Abbas et al., "MIMO Antenna System for Multi-Band Millimeter-Wave 5G and Wideband 4G Mobile Communications," *IEEE Access*, vol. 7, pp. 181916-181923, 2019. [CrossRef] [Google Scholar] [Publisher Link]

[28] Naveen Kumar, and Rajesh Khanna, "A Two Element MIMO Antenna for Sub-6 GHz and mmWave 5G Systems Using Characteristics Mode Analysis," *Microwave and Optical Technology Letters*, vol. 63, no. 2, pp. 587-595, 2021. [CrossRef] [Google Scholar] [Publisher Link]

[29] M. Habib Ullah et al., "A Dual Band Slotted Patch Antenna on Dielectric Material Substrate," *International Journal of Antennas and Propagation*, vol. 2014, pp. 1-7, 2014. [CrossRef] [Google Scholar] [Publisher Link]

[30] Vijay Sharma et al., "Super-Wideband Compact Offset Elliptical Ring Patch Antenna for 5G Applications," *Wireless Personal Communications*, vol. 122, pp. 1655-1670, 2022. [CrossRef] [Google Scholar] [Publisher Link]